Construction of Bifunctional Co/H-ZSM-5 Catalysts for the Hydrodeoxygenation of Stearic Acid to Diesel-Range Alkanes

Guangjun Wu,[a] Nan Zhang,[a] Weili Dai,[a] Naijia Guan,[a, b] and Landong Li*[a, b]

Bifunctional Co/H-ZSM-5 zeolites were prepared by a surface organometallic chemistry grafting route, namely, by the stoichiometric reaction between cobaltocene and the Brønsted acid sites in zeolites. The catalyst was applied to a model reaction of the catalytic hydrodeoxygenation of stearic acid (SA). The cobalt species existed in the form of isolated Co^{2+} ions at the exchange positions after grafting, transformed to CoO species on the surface of the zeolite, stabilized inside the zeolite channels upon calcination in air, and finally reduced by hydrogen to homogeneous clusters of metallic cobalt species approximately 1.5 nm in size. During this process, the Brønsted acid sites of the H-ZSM-5 zeolites were preserved with a slightly reduced acid strength. The as-prepared bifunctional catalyst exhibited an approximately 16 times higher activity for the hydrodeoxygenation of SA (2.11 $g_{SA} g_{cat}^{-1} h^{-1}$) than the reference catalyst (0.13 $g_{SA} g_{cat}^{-1} h^{-1}$) prepared by solid-state ion exchange and a high C_{18}/C_{17} ratio of approximately 24. The remarkable hydrodeoxygenation performance of the bifunctional Co/H-ZSM-5 was owed to the effective synergy between the uniformed metallic cobalt clusters and the Brønsted acid sites in H-ZSM-5. The simplified reaction network and kinetics of the SA hydrodeoxygenation catalyzed by the as-prepared bifunctional Co/H-ZSM-5 zeolites were also investigated.

Introduction

Triglycerides, composed of one mole of glycerol and three moles of fatty acids, are considered as high-energy density liquid molecules of biomass that can be used for the production of liquid fuels.[1] The transesterification reaction was developed as a first-generation technology for upgrading of triglycerides to fuels (bio-diesel). Typically, the transesterification process can be realized with acid or base catalysts; the process has been commercialized around the world.[1,2] Despite the advantages of biodegradability, reduced exhaust emissions, high flash point, and excellent lubricity,[3] the as-produced biodiesel shows some disadvantages such as higher oxygen content, low oxidative stability, and weak cold flow properties, which severely limit its utilization.[4]

Decarboxylation, decarbonylation, and hydrodeoxygenation (HDO) have been developed for upgrading triglycerides and fatty acid to diesel-range alkanes, namely the second-generation biofuels.[1, 2b, 5] Various types of catalysts have been investi-gated and summarized recently.[1, 2b, 6] Among these catalysts, non-noble metal catalysts such as Ni,[6c, 7] Co,[7f,g,h] W,[8] Mo,[7g] and Fe[9] are particularly attractive owing to their sufficient activity, good stability, and low price. From the view of atomic economy, the HDO process, with less C atom losses, is more desirable than the decarboxylation and decarbonylation processes for upgrading of triglycerides and fatty acids.[6d] In the HDO process, the removal of the hydroxyl group is the final step, which has been proposed to be the rate-determining step.[10] As the hydroxyl group can be easily removed on an acid site through dehydration, acidic supports are favored for the HDO process. In this context, bifunctional or multifunctional catalysts on acidic supports are preferred, which have been widely investigated for the upgrading of triglycerides and fatty acids with the HDO process.[6d, 7, 10a] Furthermore, the properties of the support materials could influence the size and distribution of the metal particles, which could significantly modulate the catalytic performance of bifunctional or multifunctional catalysts.[7a,c] Zeolites, the well-known solid acids with a high specific surface area and wide-spread industrial applications, are the most promising supports for HDO catalysts. They have been extensively investigated not only for HDO but also for other biomass upgrading processes.[6d, 11]

For bifunctional or multifunctional catalysts containing redox metal centers and acidic zeolite supports, it is most important to promote the synergy between different sites.[11] The preparation of bifunctional or multifunctional catalysts could significantly influence the synergy between different active sites and, accordingly, have a significant impact on their HDO performance. Several approaches, such as liquid/solid-state

[a] Dr. G. Wu, N. Zhang, Dr. W. Dai, Prof. N. Guan, Prof. L. Li
School of Materials Science and Engineering & National Institute for Advanced Materials
Nankai University
Tianjin 300071 (PR China)
E-mail: lild@nankai.edu.cn

[b] Prof. N. Guan, Prof. L. Li
Key Laboratory of Advanced Energy Materials Chemistry of the Ministry of Education
Collaborative Innovation Center of Chemical Science and Engineering (PR China)

The ORCID identification number(s) for the author(s) of this article can be found under:
https://doi.org/10.1002/cssc.201800670.

ion-exchange, impregnation, and deposition–precipitation, have been commonly employed for the preparation of zeolite-supported catalysts. Recently, a simple and reproducible surface organometallic chemistry (SOMC) reaction has been developed for the preparation of iron-containing zeolites.[12] Through the SOMC reaction, the iron species are grafted on the zeolite surface through the reaction between ferrocene and Brønsted acid sites in zeolites and the specific iron sites could be adjusted at the atomic and molecular level to derive well-defined catalysts for target reactions.[13]

On the basis of the above background and inspired by current achievements, herein, we report the construction of bifunctional Co/H-ZSM-5 catalysts by using the SOMC reaction and their applications in the HDO of stearic acid (SA). The properties of the cobalt species and H-ZSM-5 zeolite support are well characterized by multiple techniques and the synergy between them are clearly illustrated with catalytic data. Such a bifunctional metal/zeolite catalyst system might be extended to other complicated reactions for biomass upgrading.

Figure 1. XRD patterns of zeolite samples employed in this study.

Results and Discussion

Preparation of Co/zeolite through SOMC grafting

The physicochemical properties of the Co/zeolite samples prepared by SOMC grafting and solid-state ion exchange are summarized in Table 1. The cobalt species could be introduced in various zeolite hosts through SOMC grafting and the Co/Al ratio of approximately 1 indicated a stoichiometric reaction between cobaltocene and the Brønsted acid sites in the zeolites. No significant loss in cobalt species was observed during the subsequent calcination and reduction processes, in significant contrast to the case of Fe/zeolite.[13b] Moreover, the surface areas and pore volumes, as measured by low temperature N_2 adsorption/desorption, were well preserved during the SOMC grafting, calcination, and reduction processes (Table 1), which should be good for catalytic applications.

The XRD patterns of the Co/H-ZSM-5 samples are shown in Figure 1. Clear diffraction lines of H-ZSM-5 were observed for all samples,[14] and the diffraction lines of the cobalt species
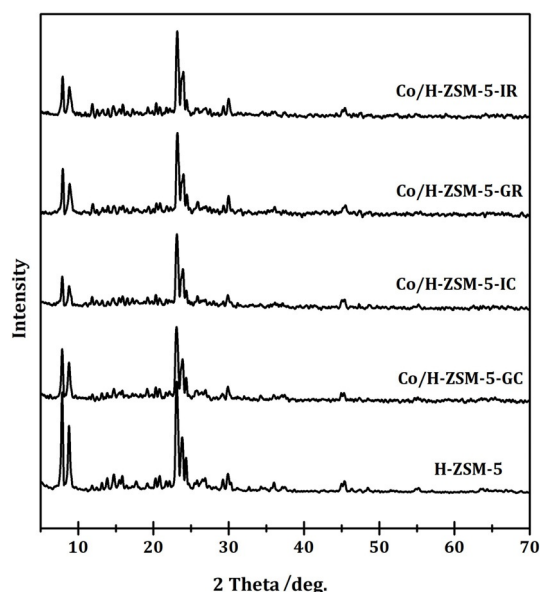
(cobalt oxides and cobalt metal) could not be distinguished owing to their low intensities and/or the overlap with the diffraction lines of the H-ZSM-5 zeolite. It could also be observed that the intensities of the diffraction lines of H-ZSM-5 zeolite decreased upon the introduction of cobalt species and subsequent calcination. Nevertheless, the framework of ZSM-5 zeolite was well preserved, consistent with the results from N_2 adsorption/desorption analyses.

FTIR spectroscopy was employed to obtain an insight of the reaction between cobaltocene and the Brønsted acid sites of H-ZSM-5, and the results are shown in Figure 2. In the hydroxyl region, three bands, that is, isolated silanol groups at 3740 cm^{-1}, hydroxyl groups bound to Lewis acid centers at 3700 cm^{-1}, and Brønsted acidic hydroxyl groups at

Table 1. Physicochemical properties of Co/zeolite samples under study.

Sample	Si/Al[a]	Co loading [%]	Co/Al[a]	S_{BET}[b] [m^2 g^{-1}]	Pore volume [cm^3 g^{-1}]
H-ZSM-5	23.7	/	/	435	0.38
Co/H-ZSM-5-G	23.9	3.93	0.95	422	0.37
Co/H-ZSM-5-GC	24.1	3.82	0.92	437	0.37
Co/H-ZSM-5-GR	24.0	3.80	0.92	439	0.37
Co/H-ZSM-5-I	23.8	4.41	1.05	403	0.36
Co/H-ZSM-5-IC	23.9	4.19	0.99	371	0.36
Co/H-ZSM-5-IR	23.8	4.25	1.00	389	0.35
Co/H-EU-1-GR	23.7	3.73	0.93	366	0.34
Co/H-mordenite-GR	23.5	4.31	1.00	392	0.41
Co/H-beta-GR	24.8	4.45	1.09	526	0.21
Co/H-USY-GR	25.3	4.08	1.04	516	0.52

[a] Molar ratio. [b] BET surface area.
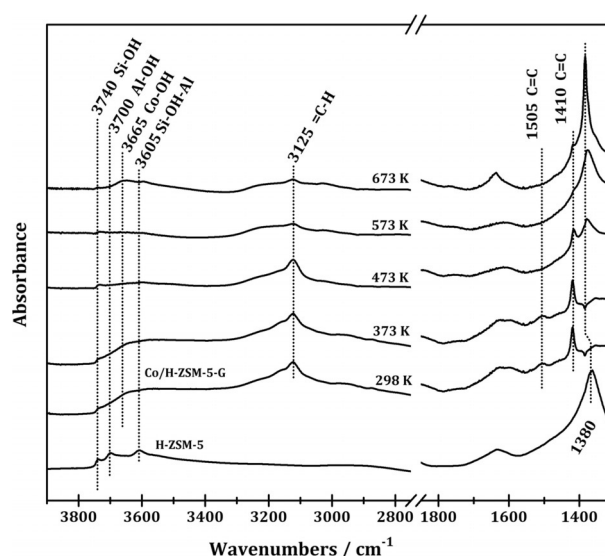
Figure 2. FTIR spectra of Co/H-ZSM-5-G at increasing temperatures.

3605 cm^{-1},[15] were observed for the parent H-ZSM-5 zeolite. Upon the introduction of cobaltocene in the zeolite through grafting, significant decreases in the intensities of the Brønsted acidic hydroxyl groups and hydroxyl groups bound to the Lewis acid centers were observed, indicating the interaction between cobaltocene and these hydroxyl groups. In addition, new bands associated with cyclopentadienyl groups appeared: The stretching vibration of =C−H at 3125 cm^{-1} and the vibrations of olefinic C=C at 1410 and 1505 cm^{-1}. These results clearly demonstrated the successful grafting of cobaltocene to the H-ZSM-5 host, which was also reflected by the change of color from white to light purple. A distinct decrease in the intensities of the IR bands attributed to the cyclopentadienyl groups was observed as the temperature was increased from 373 to 673 K, indicating the gradual removal of these groups upon thermal treatment.

The temperature-programmed reaction of Co/H-ZSM-5-G was performed and the results are shown in Figure 3. In flowing He, the decomposition of cobaltocene on H-ZSM-5 started at 423 K and the two mass fragments corresponding to C_5H_6 ($m/z = 66$) and $C_5H_5^{\cdot}$ ($m/z = 65$) were detected as the products. No cobalt-containing fragments, for example, Cp_2Co^+ ($m/z = 188$) and $CpCo^{\cdot}$ ($m/z = 124$), were observed. These results suggested that cobaltocene was stabilized on H-ZSM-5 below 423 K but decomposed at >423 K through the loss of one cyclopentadienyl group, in good agreement with the in situ FTIR results (Figure 2). In flowing O_2, CO_2 ($m/z = 44$) was detected as the exclusive product from the decomposition of cobaltocene and a two-stage CO_2 emission was observed at 553 and 703 K, respectively. It appeared that cobaltocene grafted on H-ZSM-5 was more stable in flowing O_2 than that in flowing He. According to the temperature-programmed reaction results, the organic species in Co/H-ZSM-5-G could be completely removed through calcination in flowing O_2 at 773 K and the Co/H-ZSM-5-GC sample could be successfully prepared.

Characterization of Co/H-ZSM-5

The TEM images of selected Co/H-ZSM-5 samples are shown in Figure 4. For Co/H-ZSM-5-G, clear lattice fringes of the H-ZSM-5 zeolite were observed and no cobalt species could be distinguished, although the presence of cobalt was confirmed by

energy dispersive spectroscopy analysis ($\approx 4.2\%$, not shown here). Upon the removal of the organic species through calcination at 773 K (Co/H-ZSM-5-GC), the aggregation of cobalt species did occur and tiny cobalt oxide clusters (vide infra) were observed to disperse on the surface of H-ZSM-5 and inside the channels. Subsequent reduction treatment did not result in significant changes in the size of the cobalt species and homogeneous clusters (should be metallic cobalt, vide infra) with average size of 1.5 nm were obtained for Co/H-ZSM-5-GR. In contrast, large cobalt clusters with a size of 7–20 nm were observed on the H-ZSM-5 support for Co/H-ZSM-5-IR. The TEM observations clearly demonstrated the advantage of the grafting route for obtaining homogeneous tiny cobalt clusters on a H-ZSM-5 support.

The surface states of the cobalt species in Co/H-ZSM-5-GC and Co/H-ZSM-5-IC were investigated by X-ray photoelectron spectroscopy (XPS). As shown in Figure 5, similar binding energy values at 795.1 and 779.9 eV corresponding to the $Co\,2p_{1/2}$ and $Co\,2p_{3/2}$ of Co^{3+} and/or Co^{2+}, respectively were observed for Co/H-ZSM-5-GC and Co/H-ZSM-5-IC, respectively. The satellite features at approximately 802 and 784 eV indicated the presence of Co^{2+} in these samples.[16] According to the nonlinear least-squares fitting results, Co^{2+} ions were the dominating species on H-ZSM-5 after calcination, similar to previous report on ion-exchanged Co-ZSM-5.[17]

The temperature-programmed reduction by hydrogen (H_2-TPR) profiles of Co/H-ZSM-5-GC and Co/H-ZSM-5-IC are shown in Figure 6. Typically, three hydrogen consumption peaks at approximately 500, 650, and 900 K could be clearly distinguished for both samples. According to previous H_2-TPR results on Co-ZSM-5 samples,[18] these hydrogen consumption peaks should be attributable to the reduction of CoO_x species on the surface of the zeolite, CoO_x species stabilized inside the zeolite channels, and isolated Co^{2+} ions at exchange positions, respectively. Because Co^{2+} ions were the dominating species on H-ZSM-5 (Figure 5), the total H/Co ratio of approximately 2 in the temperature range of 373–1273 K indicated the complete reduction of Co^{2+} to metallic Co. A significantly higher proportion of CoO_x species stabilized inside the zeolite channels was obtained in Co/H-ZSM-5-GC than in Co/H-ZSM-5-IC, which could originate from the different preparation methods. These CoO_x species were efficiently stabilized in the zeolite channels,
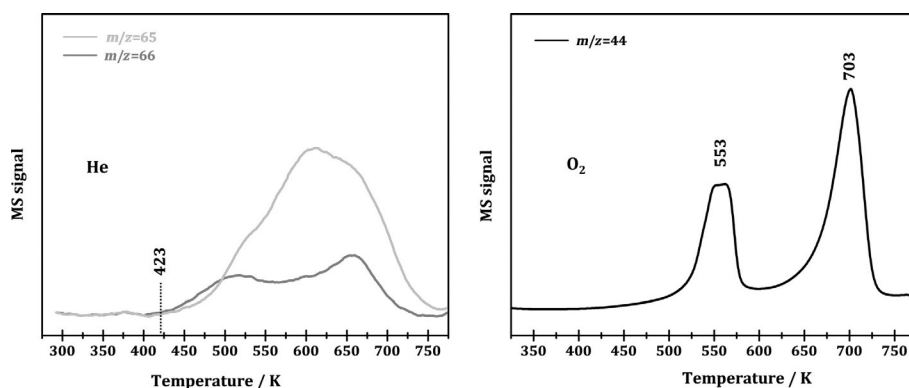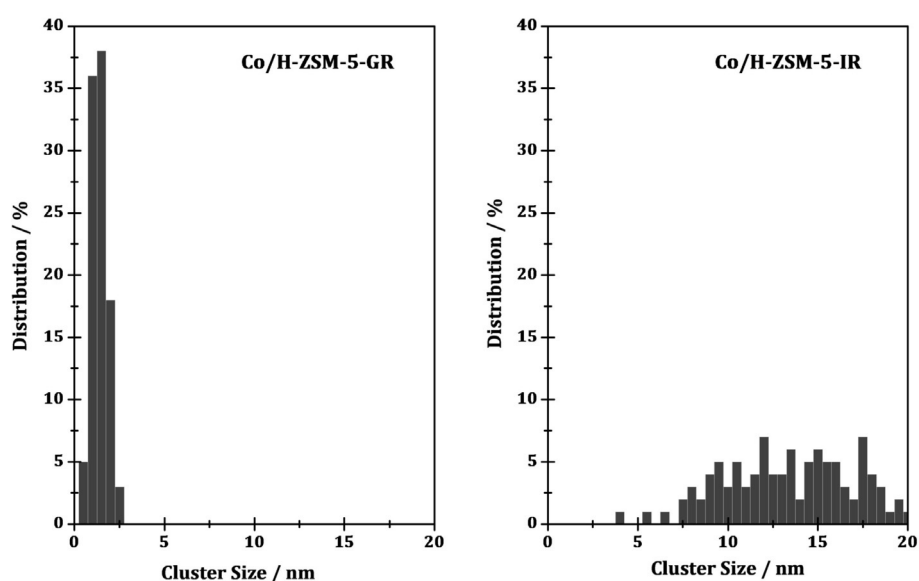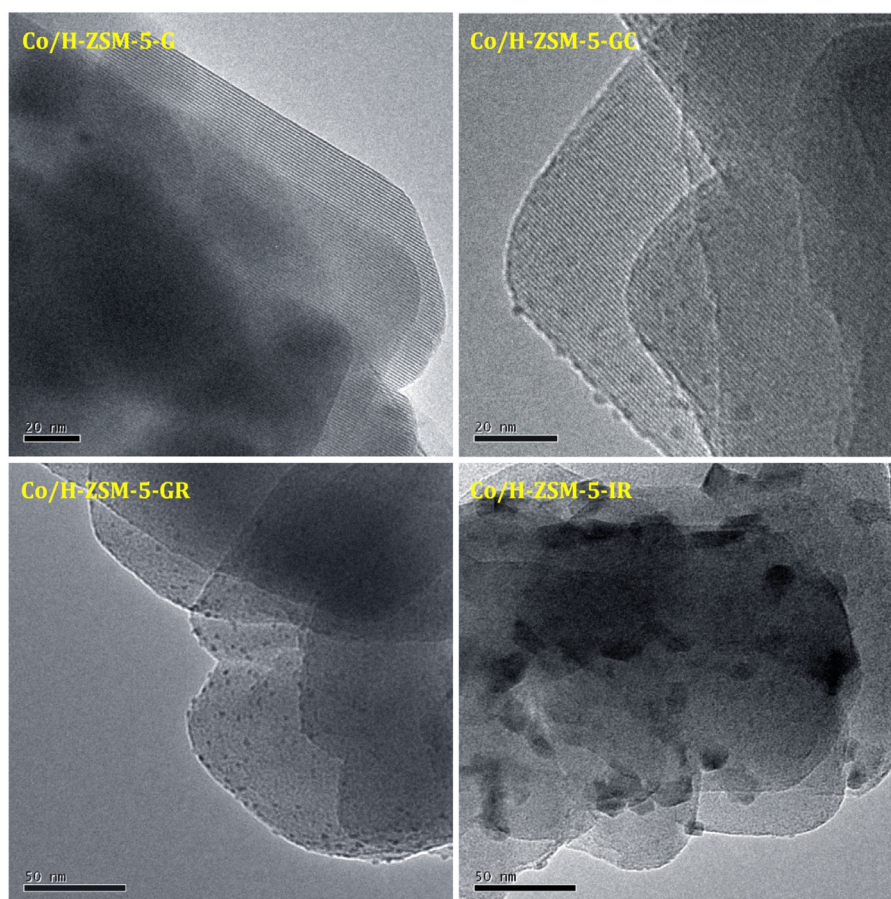

Figure 3. Temperature-programmed reaction profiles of Co/H-ZSM-5-G in flowing He or O_2.

Figure 4. TEM images of Co/H-ZSM-5-G, Co/H-ZSM-5-GC, Co/H-ZSM-5-GR, and Co/H-ZSM-5-IR; The cobalt cluster size distribution in Co/H-ZSM-5-GR and Co/H-ZSM-5-IR.

and their aggregation upon reduction was significantly suppressed, as confirmed by TEM observations (Figure 4). Our H_2-TPR results indicated that CoO_x species on the surface of the zeolite or stabilized inside the zeolite channels could be fully reduced to metallic cobalt at 773 K in flowing H_2/Ar (the typical reduction treatment conditions) whereas Co^{2+} ions at the exchange positions could not. That is, a large proportion of metallic cobalt and a small proportion of Co^{2+} ions existed in Co/H-ZSM-5-GR and Co/H-ZSM-5-IR catalysts for the HDO reaction.

The acidic properties of the Co/H-ZSM-5 zeolites were evaluated by temperature-programmed desorption of ammonia
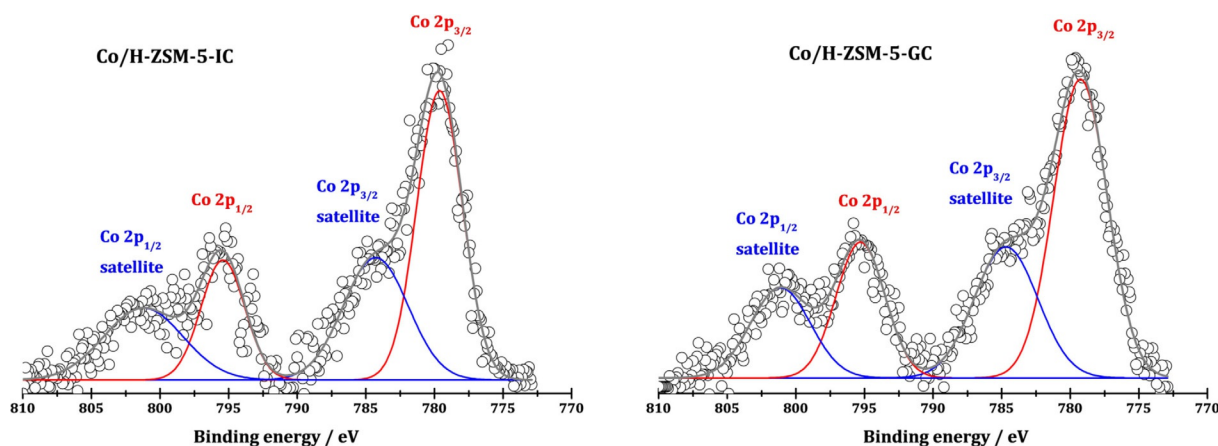
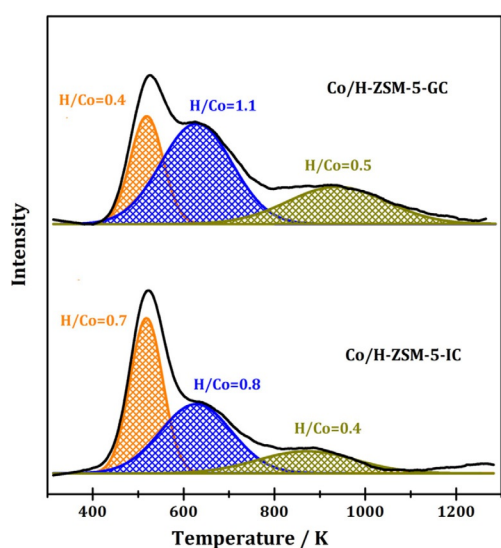**Figure 5.** Co2p XPS of Co/H-ZSM-5-GC and Co/H-ZSM-5-IC.

Figure 6. H_2-TPR profiles of Co/H-ZSM-5-GC and Co/H-ZSM-5-IC.

(NH_3-TPD) and the results are shown in Figure 7. Two ammonia desorption peaks at 493 and 743 K were observed for the parent H-ZSM-5, corresponding to the weak and strong acid sites, respectively. The high-temperature ammonia desorption peak originated from the desorption of ammonia that was strongly interacting with the Brønsted acid sites in the H-ZSM-5 zeolite.[19] With the introduction of cobalt species through SMOC grafting or solid-state ion exchange followed by calcination, the ammonia desorption peak corresponding to strong Brønsted acid sites in H-ZSM-5 disappeared, whereas a small peak centered at 673 K appeared (Figure 7, left-hand chart), which could be owed to the desorbed ammonia interacting with Lewis acidic CoO_x species (all Brønsted acid sites occupied by CoO_x species, Figure 2). The intensities of the ammonia desorption peaks at 673 K distinctly increased after reduction treatment (Figure 7, right-hand chart). The TPR analysis (Figure 6) indicated that a majority of the cobalt species in Co/H-ZSM-5-GC and Co/H-ZSM-5-IC could be reduced to metallic cobalt in flowing H_2/Ar at 773 K, accompanied by the recovery
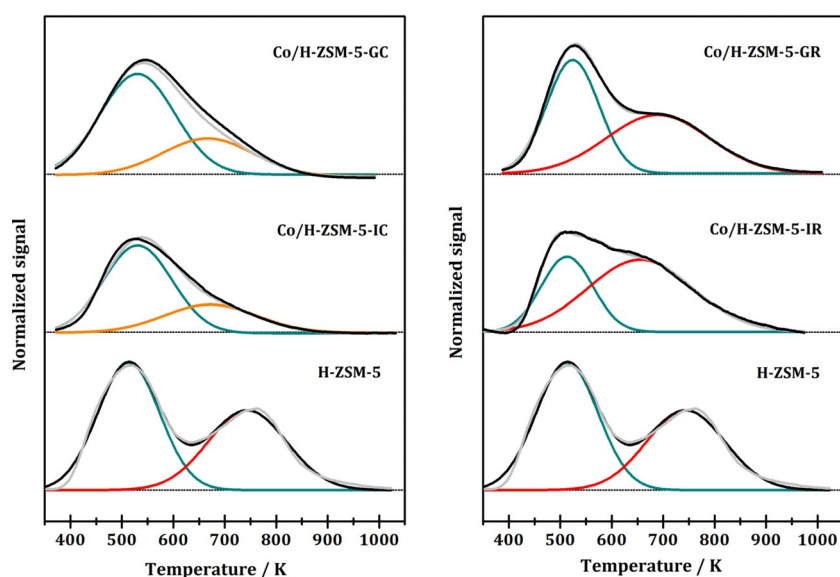

Figure 7. NH_3-TPD profiles of H-ZSM-5, Co/H-ZSM-5-IC, Co/H-ZSM-5-GC, Co/H-ZSM-5-IR, and Co/H-ZSM-5-GR.

of Brønsted acid sites in H-ZSM-5. Because the interaction between ammonia and metallic cobalt was rather weak, the ammonia desorption peak at 673 K in Co/H-ZSM-5-GR and Co/H-ZSM-5-IR mainly originated from the interaction of ammonia with the Brønsted acid sites in the H-ZSM-5 zeolite. Compared with the parent H-ZSM-5, the strength of the Brønsted acid sites in Co/H-ZSM-5-GR and Co/H-ZSM-5-IR decreased significantly, that is, the ammonia desorption peak shifted from 743 to 673 K, which could be explained by the influence of adjacent metallic cobalt species.[20]

On the basis of the above-mentioned characterization results, the cobalt species existed in the form of CoO species on the surface of the zeolite and stabilized inside the zeolite channels and isolated Co^{2+} ions at the exchange positions in Co/H-ZSM-5-GC. The majority of these cobalt species were reduced to metallic cobalt species, which appeared as homogeneous clusters of approximately 1.5 nm in Co/H-ZSM-5-GR. The Brønsted acid sites in the H-ZSM-5 could be preserved in Co/H-ZSM-5-GR whereas the acid strength was reduced to some extent. The Co/H-ZSM-5-GR was established as a bifunctional material consisting of both metallic cobalt centers and Brønsted acid sites, which should be a promising catalyst for the HDO reaction.

## Stearic acid HDO catalyzed by Co/H-ZSM-5

The catalytic HDO of SA over Co/H-ZSM-5-GR and Co/H-ZSM-5-IR was investigated, and the results are shown in Figure 8. Co/H-ZSM-5-IR exhibited very low activity in the reaction with SA, with a conversion rate of 0.13 $g_{SA} g_{cat}^{-1} h^{-1}$ at 533 K. 1-Octadecanol ($C_{18}H_{37}OH$), n-octadecane (n-$C_{18}H_{38}$), i-octadecane (i-$C_{18}H_{38}$), octadecene ($C_{18}H_{36}$), and n-heptadecane (n-$C_{17}H_{34}$) were detected as products. 1-Octadecanol was the dominant product in the early stage of the reaction. As the reaction progressed, the percentage of 1-octadecanol decreased whereas the percentage of n-octadecane increased, accompanied by the appearance of octadecene and i-octadecane. The ratio of C_{18}/C_{17} in the product was calculated to be approximately 6 after reaction for 240 min.

Co/H-ZSM-5-GR exhibited approximately 16 times higher activity (2.11 $g_{SA} g_{cat}^{-1} h^{-1}$) than Co/H-ZSM-5-IR under identical reaction conditions (0.13 $g_{SA} g_{cat}^{-1} h^{-1}$). Similar to the case of Co/H-ZSM-5-IR, 1-octadecanol was observed as the dominant product in the early stage of the reaction, which was further converted to alkanes with the progress of the reaction. The ratio of C_{18}/C_{17} in the product was approximately 24 after reaction for 240 min, in great contrast to the value of approximately 7 obtained with Co/H-ZSM-5-IR. The high SA conversion rate as well as the high C_{18}/C_{17} ratio in the product made Co/H-ZSM-5-GR a very promising nonprecious metal catalyst for the conversion of SA to diesel-range alkanes.

The HDO of SA is known to occur over bifunctional catalysts containing both acid sites and metal functional centers. In this study, both Co/H-ZSM-5-GR and Co/H-ZSM-5-IR appeared to be bifunctional catalysts containing Brønsted acid sites and cobalt centers (see characterization results). However, the cobalt particle size in Co/H-ZSM-5-GR (1.5 nm) was much smaller than that in Co/H-ZSM-5-IR (7–20 nm), which hinted at more accessible cobalt centers and a better synergy between the cobalt centers and the Brønsted acid sites in Co/H-ZSM-5-GR. These features were probably responsible for the much higher activity observed for Co/H-ZSM-5-GR in contrast to Co/H-ZSM-5-IR.

Through the SOMC grafting route, cobalt catalysts on other zeolite supports, that is, Co/H-EU-1 ($SiO_2/Al_2O_3 = 24$), Co/H-USY ($SiO_2/Al_2O_3 = 25$), Co/H-beta ($SiO_2/Al_2O_3 = 25$) and Co/H-mordenite ($SiO_2/Al_2O_3 = 25$), were prepared. These catalysts were also investigated for the HDO of SA, and the results are shown in Figure 9. Co/H-EU-1 and Co/H-mordenite exhibited remarkable activity, similar to that of Co/H-ZSM-5, whereas Co/H-USY and Co/H-Beta exhibited a lower activity. Clearly, the nature of the zeolite supports could significantly influence the catalytic activity of the cobalt catalysts, which was probably owed to the different strength and distribution of acid sites in different zeolites. Overall, Co/H-ZSM-5-GR was optimized among all Co/
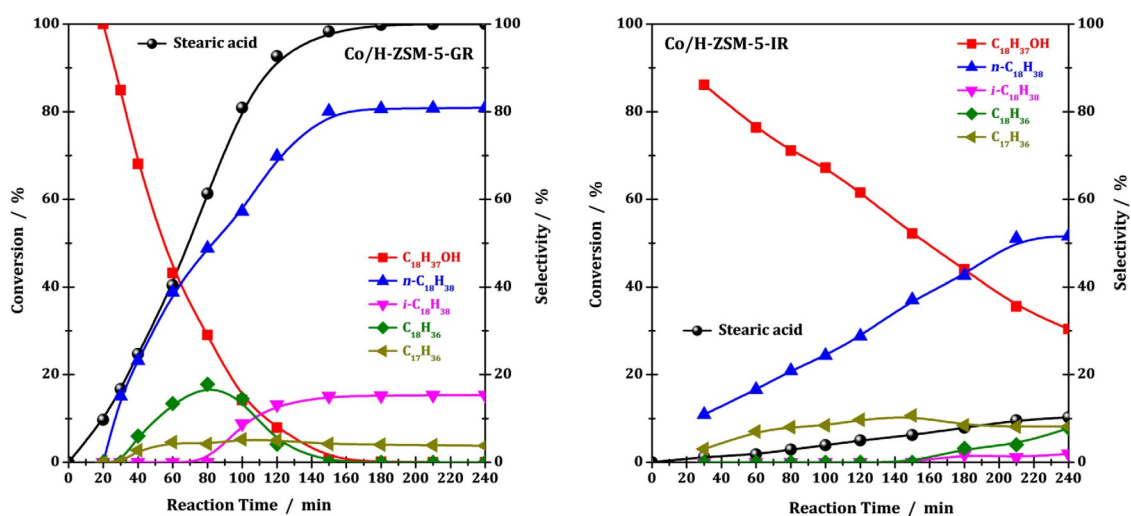
Figure 8. HDO of stearic acid over Co/H-ZSM-5-GR and Co/H-ZSM-5-IR. Reaction conditions: 1.0 g stearic acid, 100 mL n-heptane, 0.2 g catalyst, 3 MPa H_2, temperature = 533 K.
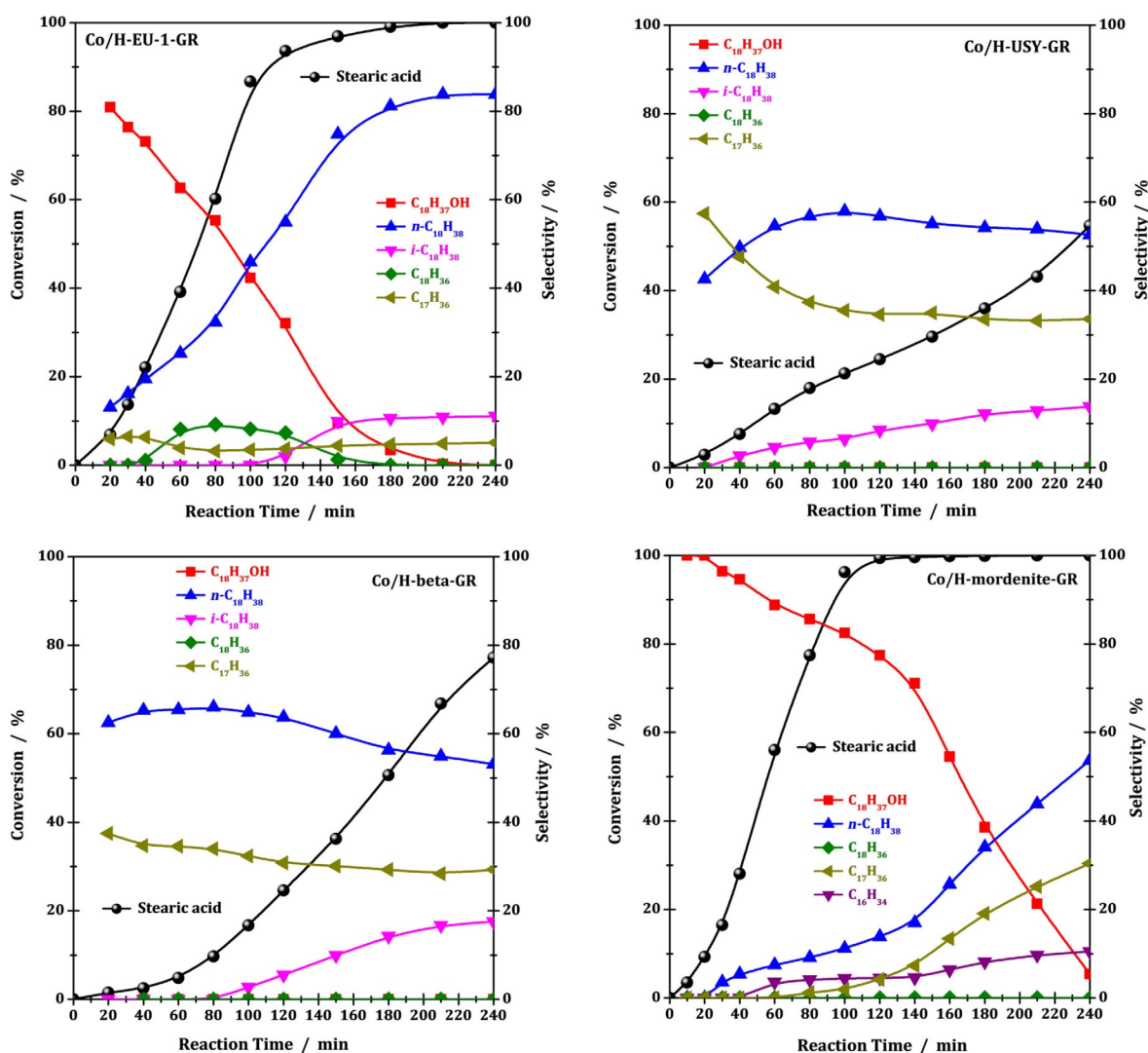
Figure 9. HDO of stearic acid over Co/zeolite-GR. Reaction conditions: 1.0 g stearic acid, 100 mL *n*-heptane, 0.2 g catalyst, 3 MPa H_2, temperature = 533 K.

zeolites investigated and was employed as a model catalyst for further kinetic study.

Reaction network and kinetics

The reaction network of SA HDO is presented in Scheme 1. SA could undergo the hydrogenation of the carbon–oxygen double bond to generate 1-octadecanol, which could be further dehydrated to octadecene. The hydrogenation of the carbon–carbon double bond in octadecene led to the formation of *n*-octadecane. Alternatively, 1-octadecanol could undergo dehydrogenation to *n*-octadecanal, which could be further converted to *n*-heptadecane through decarbonylation. For the conversion of SA to *n*-heptadecane, SA could directly undergo decarboxylation or undergo decarbonylation to heptadecene followed by hydrogenation of the carbon–carbon double bond. The intermediate product, octadecene, could be isomerized to *i*-octadecene, followed by hydrogenation to *i*-octadecane. The *n*-octadecane could also be directly isomerized to *i*-octadecane.

For the SA HDO catalyzed by Co/H-ZSM-5-GR, 1-octadecanol was the dominant product in the early stage of reaction and, therefore, the hydrogenation of the carbon–oxygen double bond in SA to 1-octadecanol was proposed as the dominant step. Afterwards, the formation and consumption of octadecene was observed (Figure 9), indicating the dehydration of 1-octadecanol to octadecene and the subsequent hydrogenation to *n*-octadecane. The relatively low amount of octadecene observed and its quick conversion revealed that the dehydration of 1-octadecanol and hydrogenation of octadecene were very fast steps. Mass spectroscopy analysis revealed that carbon monoxide was the exclusive carbon-containing gas product and, therefore, the direct decarboxylation of SA could be completely excluded. Furthermore, no heptadecene was observed in the liquid phase, excluding the possibility of decarbonylation-hydrogenation of SA to *n*-heptadecane. Therefore, the only possible pathway for the formation of *n*-heptadecane was the dehydration of 1-octadecanol followed by decarbonylation, which was in good agreement with the observation of carbon monoxide as a gas product. However, no intermediate product
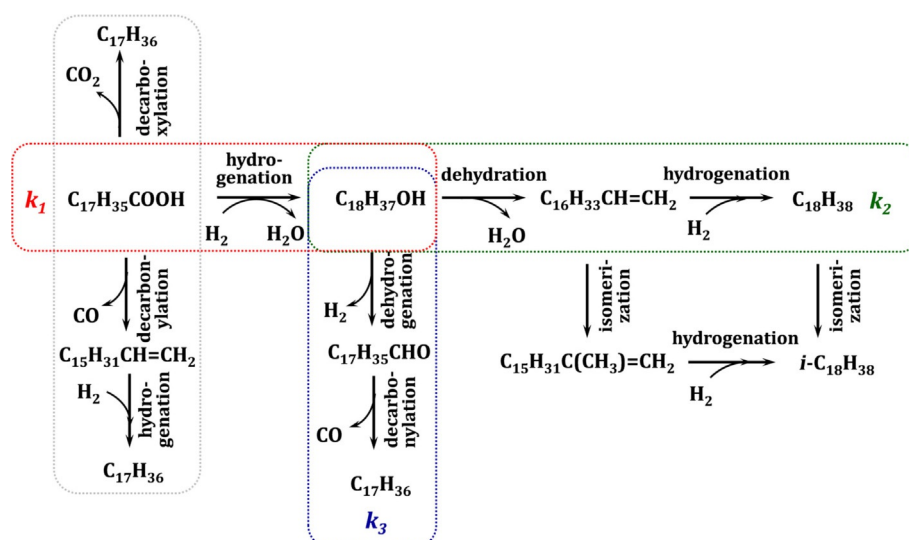
Scheme 1. Reaction network of stearic acid HDO.

n-octadecanal was detected in the liquid phase. A possible explanation was that *n*-octadecanal existed in the form of adsorbed species on the catalyst surface, which underwent very quick conversion to other products.[21]

Generally, the hydrogenation, dehydrogenation, and decarbonylation steps take place on transition metal centers, whereas the dehydration and isomerization steps occur on the Brønsted acid sites.[22] For Co/H-ZSM-5-GR, the presence of Brønsted acid sites and metallic cobalt centers as well as their effective synergy made it a robust bifunctional catalyst for SA HDO to diesel-range alkanes.

According to the reaction network in Scheme 1, an empirical kinetic model for SA HDO over Co/H-ZSM-5-GR was established. The internal diffusion of molecules inside zeolite channels could not be assessed, and, in this context, the kinetic data reported here includes the effects of internal diffusion. Furthermore, considering that the reaction was performed at a high excess of hydrogen, the effects of the gas component on the kinetic model could be ignored.[23]

Three reaction pathways were considered (Scheme 1, framed by red, green, and blue dotted line), and the conversion rates of the major products, that is, SA, 1-octadecanol ($C_{18}H_{37}OH$), octadecane ($C_{18}H_{38}$), octadecene ($C_{18}H_{36}$), and heptadecane ($C_{17}H_{36}$), were investigated according to the following equations [Eqs. (1)–(4)]:

$$\frac{dC_{SA}}{dt} = -k_1 C_{SA} \tag{1}$$

$$\frac{d(C_{C_{18}H_{38}} + C_{C_{18}H_{36}})}{dt} = k_2 C_{C_{18}H_{37}OH} \tag{2}$$

$$\frac{dC_{C_{17}H_{36}}}{dt} = k_3 C_{C_{18}H_{37}OH} \tag{3}$$

$$\frac{dC_{C_{18}H_{37}OH}}{dt} = k_1 C_{SA} - (k_2 + k_3) C_{C_{18}H_{37}OH} \tag{4}$$

HDO of SA over Co/H-ZSM-5-GR at 513–543 K was performed and the activity data are summarized in Table 2. With increasing reaction temperature, SA conversion and alkane selectivity increased whereas the 1-octadecanol selectivity decreased. On the basis of these data, the rate-constant values at different temperatures, that is, k_1, k_2, and k_3, were calculated, as shown in Table 3. The Arrhenius plots in Figure 10 revealed that the apparent activation energy value for SA conversion to 1-octadecanol was 94 kJ mol^{-1}, much lower than the conversion of 1-octadecanol to octadecane (298 kJ mol^{-1}) and heptadecane (392 kJ mol^{-1}). That is, the first hydrogenation of SA to 1-octadecanol was much easier than the further conversion of 1-octadecanol to alkanes, in good agreement with experimental observations (Figure 8). Meanwhile, the conversion of 1-oc-

Table 2. Hydrodeoxygenation of SA over Co/H-ZSM-5-GR at different temperatures.

Temperature [K]	Time [min]	SA conv. [%]	Product selectivity [%]			
			$C_{18}H_{37}OH$	$C_{18}H_{38}$	$C_{18}H_{36}$	$C_{17}H_{36}$
513	100	37.8	85.9	0.2	13.4	0.3
523	80	39.2	80.9	3.9	14.2	0.9
533	60	40.4	43.3	34.7	17.4	4.6
543	40	45.9	27.6	48.9	18.3	5.1

Table 3. Rate constants and apparent activation energy values of key pathways in the hydrodeoxygenation of stearic acid over Co/H-ZSM-5-GR.

Temperature [K]	Rate constants [s^{-1}]		
	k_1	k_2	k_3
513	1.01×10^{-4}	2.65×10^{-5}	6.38×10^{-7}
523	1.34×10^{-4}	4.67×10^{-5}	2.35×10^{-6}
533	1.88×10^{-4}	3.35×10^{-4}	2.97×10^{-5}
543	3.54×10^{-4}	1.02×10^{-3}	7.72×10^{-5}
E_a [kJ mol^{-1}]	94	298	392
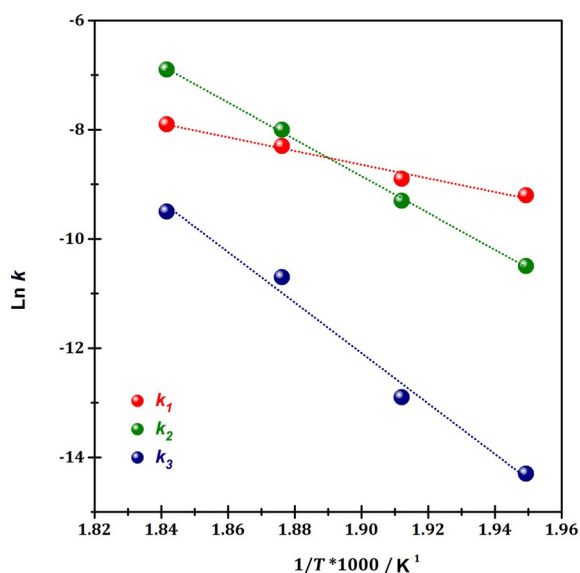
Figure 10. Arrhenius plots of different reaction pathways in SA conversion catalyzed by Co/H-SZM-5-GR.

tadecanol to heptadecane was distinctly more difficult than the conversion of 1-octadecanol to octadecane, corresponding to the lower selectivity to heptadecane than octadecane.

Conclusions

Co/H-ZSM-5 zeolites were successfully prepared through surface organometallic chemistry (SOMC) grafting, followed by calcination in air and reduction in hydrogen. TEM and temperature-programmed reduction by hydrogen (H_2-TPR) results reveal that cobalt species existed in the form of homogeneous metallic clusters of approximately 1.5 nm stabilized by zeolite, whereas the presence of Brønsted acid sites with slightly reduced acid strength compared to the parent H-ZSM-5 was confirmed by temperature-programmed desorption of ammonia (NH_3-TPD) analyses. That is, the as-prepared Co/H-ZSM-5-GR zeolites were bifunctional catalysts containing metallic cobalt clusters and Brønsted acid sites, which resulted in an effective synergy.

Co/H-ZSM-5-GR was very active in the HDO of stearic acid (SA) to diesel-range alkanes, with a reaction rate of 2.11 $g_{SA} g_{cat}^{-1} h^{-1}$, which was approximately 16 times higher than that of Co/H-ZSM-5-IR prepared through solid-state ion exchange (reaction rate of 0.13 $g_{SA} g_{cat}^{-1} h^{-1}$). Furthermore, a remarkably high C_{18}/C_{17} ratio of approximately 24 in diesel-range alkane products was achieved, indicating the neglectable carbon losses during SA conversion. Kinetic analysis results reveal that hydrogenation of SA to 1-octadecanol (with an apparent activation energy of 94 kJ mol^{-1}) was much easier than the further conversion of 1-octadecanol to alkanes, whereas the lower apparent activation energy value of the conversion of 1-octadecanol to octadecane (298 kJ mol^{-1}) than to heptadecane (392 kJ mol^{-1}) explained the high ratio of C_{18}/C_{17} in the diesel-range alkane products.

Experimental Section

Catalyst preparation

Alumino-silicate zeolites in their H-form with a similar SiO_2/Al_2O_3 ratio of 25, that is, H-ZSM-5, H-EU-1, H-USY, and H-modenite, were provided by Sinopec and employed as supports for the cobalt species. Co/zeolite samples were prepared by an organometallic grafting method.[12] During the grafting process, the organometallic cobalt precursor cobaltocene (Cp_2Co) sublimed at elevated temperature and then reacted with the Brønsted acid sites in the zeolites. In a typical experiment, a zeolite sample of 2.5 g was placed in a quartz reaction chamber connected to a vacuum line and treated under a vacuum of 5×10^{-2} Pa at 573 K for 4 h. After cooling to 323 K, 0.5 g cobaltocene was added into the reaction chamber, which was heated to and kept at 423 K under vacuum for 24 h to ensure the complete surface reaction between cobaltocene and the Brønsted acid sites in the zeolites. The resulting solid (labelled as Co/zeolite-G) was subjected to calcination in flowing air at 773 K for 6 h and labelled as Co/zeolite-GC. The Co/zeolite-GC sample was further subjected to reduction in flowing 10%H_2/Ar at 773 K for 6 h and then labelled as Co/zeolite-GR.

For reference, the Co/H-ZSM-5 sample was also prepared by solid-state ion exchange. In a typical experiment, 2.5 g H-ZSM-5 zeolite was mechanically mixed with 0.5 g cobalt acetate in a glove box and the mixture was placed in a sealed reactor. The reactor was heated to and kept at 573 K for 2 h. The resulting solid was thoroughly washed with deionized water, dried at 353 K overnight (labelled as Co/H-ZSM-5-I), calcined in flowing air at 773 K for 6 h, and labelled as Co/H-ZSM-5-IC. The Co/zeolite-IC sample was further subjected to reduction in flowing 10%H_2/Ar at 773 K for 6 h and then labelled as Co/zeolite-IR.

Characterization techniques

The exact cobalt loadings in the Co/zeolite samples were determined on an IRIS Advantage inductively coupled plasma atomic emission spectrometer (ICP-AES). The specific surface areas and pore volumes of the samples were determined through N_2 adsorption/desorption isotherms at 77 K collected on a Quantachrome iQ-MP gas adsorption analyzer. The XRD patterns of the Co/zeolite samples were recorded on a Bruker D8 ADVANCE powder diffractometer using CuK_α radiation ($\lambda=0.1542$ nm) at a scanning rate of 4° min^{-1} in the region of $2\theta=5$–50°. The TEM images of the samples were taken on a FEI Tecnai G^2 F20 electron microscope at an acceleration voltage of 200 kV. A few drops of an alcohol suspension containing the sample were placed on a carbon-coated copper grid, followed by evaporation at ambient temperature. The FTIR spectra of Co/H-ZSM-5-G in flowing He were measured on a Bruker Tensor 27 spectrometer with 128 scans at a resolution of 2 cm^{-1}. A self-supporting pellet made from the sample was placed in the reaction chamber and heated to the designed temperatures for recording the spectrum. The temperature-programmed reaction of Co/H-ZSM-5-G in flowing He or O_2 was performed on quartz tube reactor and the products were analyzed on-line by a Pfeiffer Omnistar GSD 320 mass spectrometer. The XPS spectra of the Co/zeolite samples were recorded on a Kratos Axis Ultra DLD spectrometer with a monochromated AlK_α X-ray source ($h\nu=$ 1486.6 eV), hybrid (magnetic/electrostatic) optics, and a multichannel plate and delay line detector. All spectra were recorded by using an aperture slot of 300×700 µm. Accurate binding energies (±0.1 eV) were determined with respect to the position of the adventitious C 1s peak at 284.8 eV. The NH_3-TPD experiments were performed on a Quantachrome ChemBET 3000 chemisorption ana-

lyzer. A sample of approximately 0.1 g was pretreated in flowing He at 673 K for 1 h, cooled to 373 K in He and saturated with 5% NH_3/He. After that, the sample was purged with He for 30 min to eliminate the physisorbed ammonia. NH_3-TPD was then performed in flowing He in the temperature range of 373–1073 K at a heating rate of 10 K min^{-1}. The H_2-TPR of the samples was performed on a chemisorption analyzer (Quantachrome ChemBET 3000) with 10% H_2/Ar at a heating rate of 10 K min^{-1} from 373 to 1273 K. Prior to reduction, the sample (100 mg) was calcined in dry air at 673 K for 1 h.

Catalytic reaction and product analysis

The HDO of SA (Adamas, 99%) was performed in a high-pressure stainless autoclave (Xinyuan Chemical Machinery, Series CJK, 300 mL) at a stirring rate of 750 rpm (adequate to exclude the external diffusion limitations). In a typical experiment, 0.2 g catalyst, 1.0 g SA, and 100 mL n-heptane were mixed well in the autoclave and purged with pure N_2 at room temperature. The autoclave was rapidly heated to the desired temperature and H_2 was introduced at 3.0 MPa to initiate the reaction.

After the reaction, the liquid organic products were analyzed by gas chromatography (Shimadzu GC-2010) and gas chromatography-mass spectrometry (Shimadzu GCMS-QP2010 SE), both with a RXI-5MS column (30 m, 0.25 mm i.d., stationary phase thickness 0.25 μm). Eicosane was used as an internal standard for quantification. The following temperature program was employed: Isothermal heating at 323 K for 5 min, heating to 573 K at a rate of 10 K min^{-1}, and isothermal heating at 573 K for 10 min. The gas products were qualitatively analyzed with a mass spectrometer (Pfeiffer Omnistar GSD 320).

Conflict of interest

The authors declare no conflict of interest.

[1] G. W. Huber, S. Iborra, A. Corma, Chem. Rev. 2006, 106, 4044–4098.

[2] a) R. G. Bray, Biodiesel Production, SRI Consulting, 2004; b) B. Ma, J. Zhang, H. Cui, M. He, C. Zhao, Sci. Sin. Chim. 2015, 45, 350–360.

[3] G. Knothe in The Biodiesel Handbook, 2nd ed. (Eds.: G. Knothe, J. Krahl, J. V. Gerpen), AOCS Press, Urbana, Illinois, 2005, pp. 1–3.

[4] P. Šimáček, D. Kubička, G. Šebor, M. Pospíšil, Fuel 2009, 88, 456–460.

[5] a) S. Foraita, Y. Liu, G. L. Haller, E, Baráth, C. Zhao, J. A. Lercher, ChemCatChem 2017, 9, 195–203; b) G. Xu, Y. Zhang, Y. Fu, Q. Guo, ACS Catal. 2017, 7, 1158–1169.

[6] a) M. Saidi, F. Samimi, D. Karimipourfard, T. Nimmanwudipong, B. C. Gates, M. R. Rahimpour, Energy Environ. Sci. 2014, 7, 103–129; b) K. A. Rogers, Y. Zheng, ChemSusChem 2016, 9, 1750–1772; c) C. Kordulis, K. Bourikas, M. Gousi, E. Kordouli, A. Lycourghiotis, Appl. Catal. B 2016,

181, 156–196; d) Y. Shi, E. Xing, K. Wu, J. Wang, M. Yang, Y. Wu, Catal. Sci. Technol. 2017, 7, 2385–2415; e) X. Li, X. Luo, Y. Jin, J. Li, H. Zhang, A. Zhang, J. Xie, Renewable Sustainable Energy Rev. 2018, 82, 3762–3797; f) Y. Wang, S. De, N. Yan, Chem. Commun. 2016, 52, 6210–6224.

[7] a) B. Peng, Y. Yao, C. Zhao, J. A. Lercher, Angew. Chem. Int. Ed. 2012, 51, 2072–2075; Angew. Chem. 2012, 124, 2114–2117; b) B. Peng, X. Yuan, C. Zhao, J. A. Lercher, J. Am. Chem. Soc. 2012, 134, 9400–9405; c) B. Ma, C. Zhao, Green Chem. 2015, 17, 1692–1701; d) I. Hachemi, N. Kumar, P. Mäki-Arvela, J. Roine, M. Peurla, J. Hemming, J. Salonen, D. Y. Murzin, J. Catal. 2017, 347, 205–221; e) B. Ma, H. Cui, D. Wang, P. Wu, C. Zhao, Nanoscale 2017, 9, 5986–5995; f) A. Srifa, N. Viriya-empikul, S. Assabumrungrat, K. Faungnawakij, Catal. Sci. Technol. 2015, 5, 3693–3705; g) V. K. Soni, P. R. Sharma, G. Choudhary, S. Pandey, R. K. Sharma, ACS Sustainable Chem. Eng. 2017, 5, 5351–5359; h) Y. Shi, E. Xing, Y. Cao, M. Liu, K. Wu, M. Yang, Y. Wu, Chem. Eng. Sci. 2017, 166, 262–273; i) W. Li, Y. Gao, S. Yao, D. Ma, N. Yan, Green Chem. 2015, 17, 4198–4205.

[8] a) R. W. Gosselink, D. R. Stellwagen, J. H. Bitter, Angew. Chem. Int. Ed. 2013, 52, 5089–5092; Angew. Chem. 2013, 125, 5193–5196; b) S. A. W. Hollak, R. W. Gosselink, D. S. van Es, J. H. Bitter, ACS Catal. 2013, 3, 2837–2844.

[9] K. Kandel, J. W. Anderegg, N. C. Nelson, U. Chaudhary, I. I. Slowing, J. Catal. 2014, 314, 142–148.

[10] a) B. Peng, C. Zhao, S. Kasakov, S. Foraita, J. A. Lercher, Chem. Eur. J. 2013, 19, 4732–4741; b) B. Rozmysłowicz, P. Mäki-Arvela, A. Tokarev, A.-R. Leino, K. Eränen, D. Y. Murzin, Ind. Eng. Chem. Res. 2012, 51, 8922–8927.

[11] T. Ennaert, J. V. Aelst, J. Dijkmans, R. D. Clercq, W. Schutyser, M. Dusselier, D. Verboekend, B. F. Sels, Chem. Soc. Rev. 2016, 45, 584–611.

[12] a) J. Long, X. Wang, G. Zhang, J. Dong, T. Yan, Z. Li, X. Fu, Chem. Eur. J. 2007, 13, 7890–7899; b) J. Long, X. Wang, Z. Ding, Z. Zhang, H. Lin, W. Dai, X. Fu, J. Catal. 2009, 264, 163–174.

[13] a) X. Wang, J. Long, G. Yan, G. Zhang, X. Fu, Microporous Mesoporous Mater. 2008, 108, 258–265; b) G. Wu, F. Hei, N. Zhang, N. Guan, L. Li, W. Grünert, Appl. Catal. A 2013, 468, 230–239.

[14] M. M. J. Treacy, J. B. Higgins, Collection of simulated XRD powder patterns for zeolites (Fifth Revised Edition), Elsevier, Amsterdam, 2007, pp. 276–279.

[15] G. Wu, F. Hei, N. Guan, L. Li, Catal. Sci. Technol. 2013, 3, 1333–1342.

[16] http://www.xps-simplified.com/periodictable.php.

[17] T. Sun, M. L. Trudeau, J. Y. Ying, J. Phys. Chem. 1996, 100, 13662–13666.

[18] a) E. van Steen, G. S. Sewell, R. A. Makhothe, C. Micklethwaite, H. Manstein, M. de Lange, C. T. O'Connor, J. Catal. 1996, 162, 220–229; b) X. Wang, H. Chen, W. M. H. Sachtler, Appl. Catal. B 2000, 26, L227–L239; c) X. Wang, H. Chen, W. M. H. Sachtler, Appl. Catal. B 2001, 29, 47–60; d) A. Martínez-Hernández, G. A. Fuentes, Appl. Catal. B 2005, 57, 167–174.

[19] a) L. J. Lobree, I. C. Hwang, J. A. Reimer, A. T. Bell, J. Catal. 1999, 186, 242–253; b) M. Iwasaki, K. Yamazaki, K. Banno, H. Shinjoh, J. Catal. 2008, 260, 205–216.

[20] D. Santi, S. Rabl, V. Calemma, M. Dyballa, M. Hunger, J. Weitkamp, ChemCatChem 2013, 5, 1524–1530.

[21] a) L. Di, S. Yao, M. Li, G. Wu, W. Dai, G. Wang, L. Li, N. Guan, ACS Catal. 2015, 5, 7199–7207; b) L. Di, S. Yao, G. Wu, W. Dai, N. Guan, L. Li, Appl. Catal. B 2017, 201, 137–149.

[22] a) P. Kumar, S. R. Yenumala, S. K. Maity, D. Shee, Appl. Catal. A 2014, 471, 28–38; b) L. Boda, G. Onyestyak, H. Solt, F. Lonyi, J. Valyon, A. Thernesz, Appl. Catal. A 2010, 374, 158–169; c) M. Besson, P. Gallezot, C. Pinel, Chem. Rev. 2014, 114, 1827–1870; d) G. Yao, G. Wu, W. Dai, N. Guan, L. Li, Fuel 2015, 150, 175–183.

[23] J. Lin, T. A. Trabold, M. R. Walluk, D. F. Smith, Int. J. Hydrogen Energy 2014, 39, 183–195.